Response of Morris-Lecar neurons to various stimuli

Hengtong Wang, Longfei Wang, Lianchun Yu, and Yong Chen*
Institute of Theoretical Physics, Lanzhou University, Lanzhou 730000, China
(Received 24 September 2010; revised manuscript received 19 December 2010; published 24 February 2011)

We studied the responses of three classes of Morris-Lecar neurons to sinusoidal inputs and synaptic pulselike stimuli with deterministic and random interspike intervals (ISIs). It was found that the responses of the output frequency of class 1 and 2 neurons showed similar evolution properties by varying input amplitudes and frequencies, whereas class 3 neuron exhibited substantially different properties. Specifically, class 1 and 2 neurons display complicated phase locking ($p:q$, $p > q$, denoting output action potentials per input spikes) in low-frequency sinusoidal input area when the input amplitude is above their threshold, but a class 3 neuron does not fire action potentials in this area even if the amplitude is much higher. In the case of the deterministic ISI synaptic injection, all the three classes of neurons oscillate spikes with an arbitrary small frequency. When increasing the input frequency (both sinusoidal and deterministic ISI synaptic inputs), all neurons display $1:1$ phase locking, whereas the response frequency decreases even fall to zero in the high-frequency input area. When the random ISI synaptic pulselike stimuli are injected into the neurons, one can clearly see the low-pass filter behaviors from the return map. The output ISI distribution depends on the mean ISI of input train as well as the ISI variation. Such different responses of three classes of neurons result from their distinct dynamical mechanisms of action potential initiation. It was suggested that the intrinsic dynamical cellular properties are very important to neuron information processing.

DOI: 10.1103/PhysRevE.83.021915 PACS number(s): 87.19.ll, 87.19.ls, 05.45.Xt

I. INTRODUCTION

Under certain forms of external stimulus, neurons can fire action potentials (spikes), which are known to be responsible for transmitting information in the nervous system [1,2]. The ability of neurons to encode and decode the characteristics of presynaptic stimuli enables the flow of information within our brains. For decades, many influential coding schemes were proposed, such as rate coding (the average number of spikes per unit time), temporal coding (the precise timing of single spike), and population coding (encoding information by the joint activities of a large number of neurons) [3–5]. There is now a consensus that different neural systems may resort to different coding strategies. Moreover, recent studies also suggested the possibility of dual or multiple coding mechanisms [6,7]. What kinds of coding schemes are used in nervous systems is a topic of intense debate within the neuroscience community. On the other hand, neurons exist in many different shapes and sizes and can be classified by their morphology and function [8]. Different neurons play different roles in information processing and transmission. While the precise coding recipe in the nervous system is uncertain, the responses of various classes of neurons to different stimuli are fundamental to understanding information transfer in the nervous system.

From the electrophysiological characteristics of neurons, Hodgkin identified three basic classes of neurons distinguished by their frequency-current (f-I) relationship [9–13]. Class 1 neurons generate action potentials with an arbitrary low frequency in response to weak stimulation with a continuous f-I curve. Class 2 neurons fire spikes within a certain frequency band with a discontinuous f-I curve. Class 3 neurons, however, fail to spike repetitively, and typically spike only one time at the onset of stimulation.

However, knowing the f-I relationship is not enough to predict neuronal responses to time-varying inputs. Recently, numerous studies have been carried out in the area of class 1 or 2 neurons under a stimuli with the form of a constant direct current plus a sinusoidal term. With the variation in the amplitude or the frequency of the input stimuli, the neuronal response produces complex phase-locking and chaotic behaviors [14–17]. It was also reported that these behaviors were observed in cortical neurons *in vivo* [18]. When interneurons or pyramidal neurons were subjected to sinusoidal stimulation, the firing threshold rises sharply at a high value of input frequency, showing bandpass-filter behavior [19]. Numerical studies also shown that various bifurcations including inverse flip period doubling and saddle-node bifurcations form the boundaries of complicated mode-locking structures [20]. The response of a Hodgkin-Huxley neuron (class 2 neuron) to a high-frequency input is irregular, and the output interspike interval histogram undergoes a sharp transition [21].

In spite of the wealth of the studies on firing properties of neurons, the discussions of former works were limited to class 1 (Integrate-and-Fire Model) or class 2 (Hodgkin-Huxley model) neurons, and there have been few discussions about the differences between the two neuron classes. Class 3 neurons and the different properties among the three classes of neurons have never been discussed in this respect. In our present work, using a modified Morris-Lecar (ML) model, we numerically investigated the response of three kinds of Hodgkin-classified neurons with different time-varying inputs. This modified ML model could exhibit all three excitabilities. We not only discuss the responses of the three classes of neurons to those different types of inputs, but also analyze the difference of the response properties among the three classes. First, an external stimulus was set to be sinusoidal in form.

*ychen@lzu.edu.cn

 ©2011 American Physical Society

Then a simulated synaptic input with deterministic interspike intervals (ISIs) was chosen as an external stimulus. Finally, we employed a synaptic input with a random ISI distribution. Our results revealed that the output frequencies of class 1 and 2 neurons show similar evolution properties, but that of class 3 neurons exhibit different behaviors. Neurons show interesting phase-locking behaviors, and their response frequency can increase or decrease as the stimulus frequency increases. The output of the ISI distribution depends on the mean ISIs of inputs as well as their variations.

Our paper is organized as follows. In Sec. II, we give a simple description of the neuron model with three kinds of responses. In Sec. III, we show the result of response of three classes of neurons to sinusoidal input, time-dependent synaptic input, and random synaptic input. The conclusion is given in Sec. IV.

II. MODEL

In our numerical study, we utilize a modified ML model [12]. Varying a single parameter, this model exhibits all three excitabilities. This system is described by the following equations:

$$C dV/dt = -g_{\text{fast}} m(V)(V - E_{\text{Na}}) - g_{\text{slow}} W(V - E_K) - g_{\text{leak}}(V - E_{\text{leak}}) + I_{\text{ext}}, \quad (1)$$

$$dW/dt = \phi \frac{W_\infty(V) - W}{\tau(V)}, \quad (2)$$

$$m(V) = 0.5\left[1 + \tanh\left(\frac{V - \beta_m}{\gamma_w}\right)\right], \quad (3)$$

$$W_\infty(V) = \left[1 + \tanh\left(\frac{V - \beta_w}{\gamma_w}\right)\right], \quad (4)$$

$$\tau(V) = 1/\cosh\left(\frac{V - \beta_w}{2\gamma_w}\right). \quad (5)$$

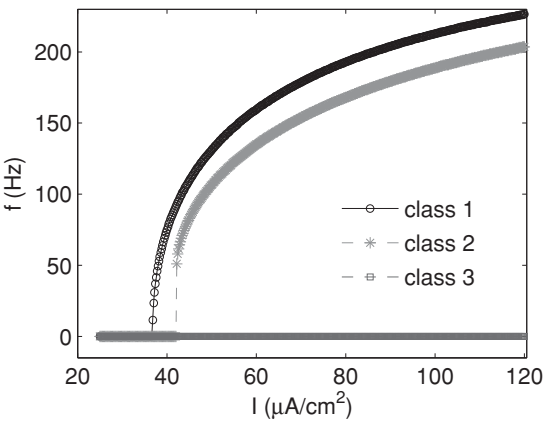

FIG. 1. Frequency-current (f-I) curves of three classes of excitabilities computed by Eqs. (1)–(5) with sustained external injecting direct currents I_{ext} of varying amplitude. Class 1 neurons have a continuous f-I curve (upper), whereas the curve of class 2 neurons is discontinuous (middle). Here the frequency of class 3 neurons is zero, because the measurement of firing rate requires at least two spikes (bottom).

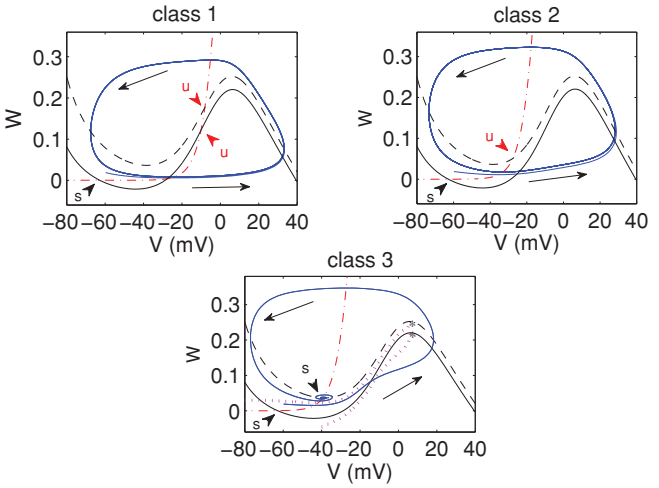

FIG. 2. (Color online) Phase planes of the membrane potential V plotted against the slower recovery variable W. The intersection points of V nullcline (subthreshold stimuli, black solid; upper threshold, stimuli black dash) and W nullcline (red dash-dot) represent stable(black arrowhead) or unstable fixed points (red arrowhead). Upper-threshold DC stimulus shifts the V nullcline upward (black dash), destroying or displacing the former fixed points, thereby allowing the neuron to spike. The direction of trajectories (blue solid) is indicated by black arrows. The two pink dotted lines in the bottom panel present quasiseparatrixes, and the asterisk denotes the head of the quasiseparatrix.

Here V is the membrane potential, and W is a slower recovery variable. The term $-g_{\text{fast}} m(V)(V - E_{\text{mNa}})$ denotes a fast Na^+ current, $-g_{\text{slow}} W(V - E_K)$ denotes a slow K^+ current, and $-g_{\text{leak}}(V - E_{\text{leak}})$ is a leak current. The parameter values are $E_{\text{Na}} = 50$ mV, $E_K = -100$ mV, $E_{\text{leak}} = -70$ mV, $g_{\text{fast}} = 20$ mS/cm^2, $g_{\text{slow}} = 20$ mS/cm^2, $g_{\text{leak}} = 2$ mS/cm^2, $\phi = 0.15$, $C = 2\mu$ F/cm^2, $\beta_m = -1.2$ mV, $\gamma_m = 18$ mV, and $\gamma_w = 10$ mV. Hereβ_w is identified as a varying parameter. In our study, we chose $\beta_w = 0$ mV (class 1 excitability), -13 mV (class 2 excitability), and -23 mV (class 3 excitability). I_{ext} is the external input current with different forms in our work. Figure 1 shows the f-I curve of each of the three excitabilities. Note that the frequency of class 3 neurons is undefined, for the measurement of firing rate requires at least two spikes, and class 3 neurons fire at most once.

As stated in Ref. [12], the spike-initiating dynamics of the three excitabilities represent different outcomes in nonlinear competition between oppositely directed kinetically mismatched currents. Class 1 excitability occurs through a saddle-node bifurcation, class 2 excitability occurs through a Hopf bifurcation, and class 3 excitability occurs through a quasiseparatrix crossing. Figure 2 gives the phase planes of three classes of neurons excited by a suprathreshold direct current (DC).

III. SIMULATION RESULTS AND DISCUSSIONS

A. Sinusoidal input

First, we focus on the response of ML neurons to sinusoidal external inputs. The sinusoidal input I_{ext} is given by

$$I_{\text{ext}} = A_{\text{in}} \sin(2\pi f_{\text{in}} t), \quad (6)$$

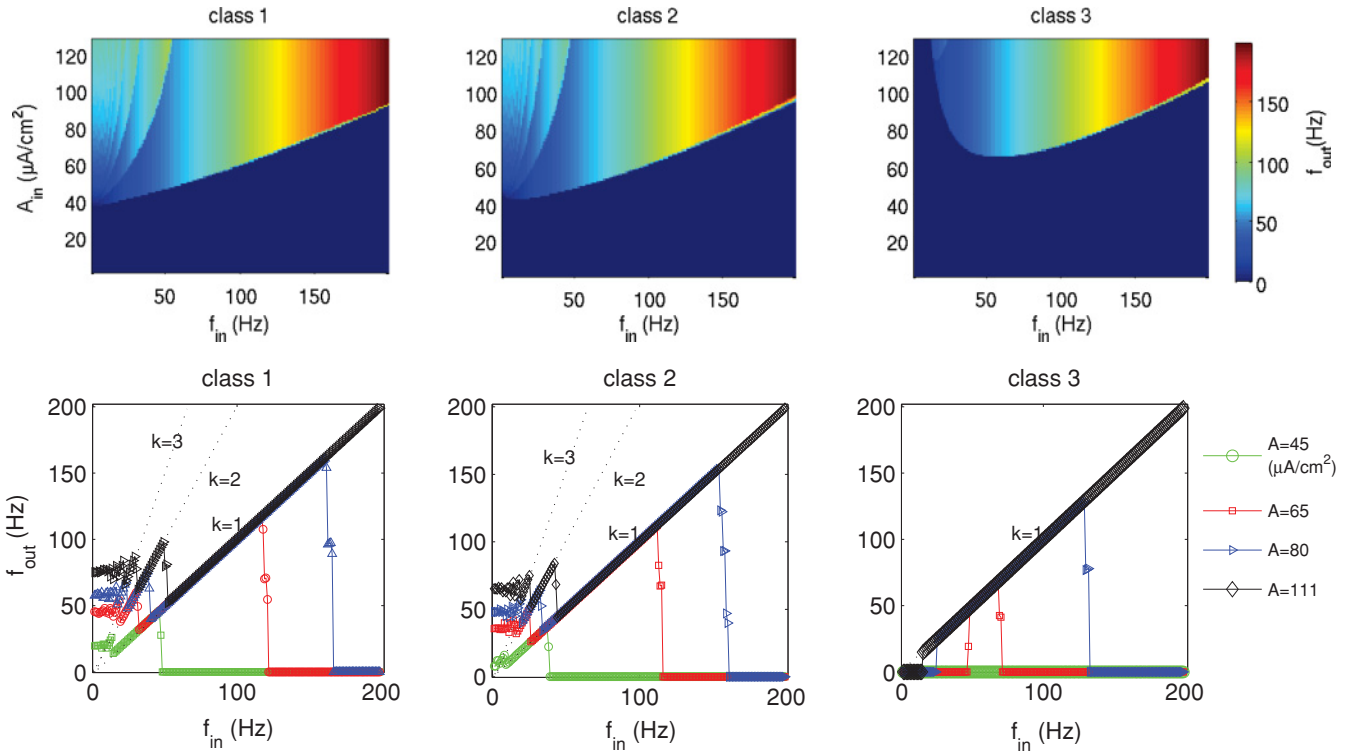

FIG. 3. (Color online) The average output frequency f_{out} of the three classes of neurons as a function of the sinusoidal input frequency f_{in} and amplitude A_{in}. Dotted curves in bottom panels denote $k = f_{\text{out}}/f_{\text{in}}$.

where A_{in} is input amplitude and f_{in} is input frequency. A_{in} and f_{in} are set as free parameters.

The average output frequency in the form of a color map as a function of the input frequency and amplitude is shown in Fig. 3 (top panels). The color marks the average output firing frequency f_{out} of the neurons during our stimulation (not less than 10 s). The output frequency patterns of class 1 and 2 neurons are similar, whereas class 3 neurons show a different pattern. In the case of high input frequency, a higher input amplitude is needed to activate the neurons. That is to say, the threshold of three classes of neurons increases with the increasing of input frequency. In the low-frequency stimuli area, the output firing rate of class 1 and 2 neurons is discontinuous as the input frequency increases. The low-frequency parameter space of class 1 and 2 neurons was divided into many sector areas. The ratio of the output frequency to input frequency is the same in the same sector area. Class 3 neurons do not respond to the low-frequency input even if the input amplitude is very high.

To show the details of the response behaviors of three classes of neurons to sinusoidal stimuli, the evolution of output frequency f_{out} with the input frequency f_{in} is plotted in the bottom panels of Fig. 3. Here dotted curves denote $k = f_{\text{out}}/f_{\text{in}}$. Under slow sine-wave stimuli, class 1 and 2 neurons have a higher output frequency than their input frequency, and f_{out} increases with different slopes (dotted line) by changing f_{in}. Class 1 and 2 neurons display $p:q$ ($p > q$) phase locking (bursting, Fig. 4) behaviors, and the phase-locking firing patterns transform frequently in the low-input-frequency area.

Class 3 neurons require inputs with higher amplitude and frequency to fire action potentials. When f_{in} increases, f_{out} of all neurons produce $1:1$ phase locking. When further increasing f_{in}, all the neurons exhibit subthreshold oscillation, and the action potential vanishes. As the amplitude of the input sine wave increases, the range of $1:1$ phase-locking state is extended for all three classes.

Neurons display different behaviors due to their dynamical mechanisms of action potential initiation. The sinusoidal input has a rising phase (mainly contributing to depolarization effect) and falling phase (mainly contributing to polarization or the hyperpolarization effect). Under periodic stimuli, the fixed points in the quiescent state are destroyed, and the

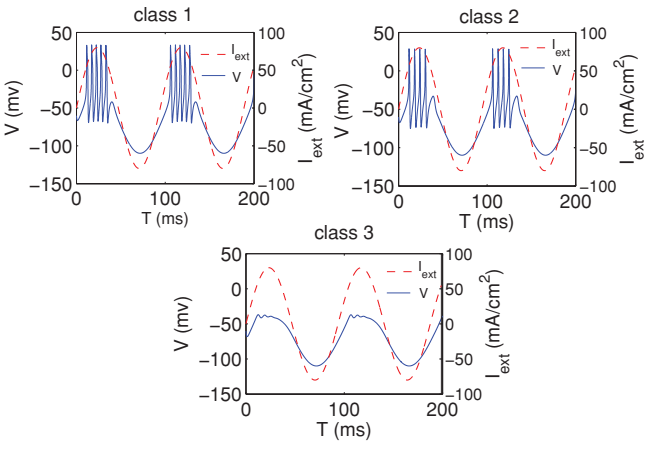

FIG. 4. (Color online) The bursting behaviors of class 1 and 2 neurons. The dashed red line denotes the input current, and the solid blue line denotes membrane potential.

membrane potential begins to oscillate. When a low-frequency sinusoidal current is injected into class 1 and 2 neurons, the two excitabilities are triggered through the saddle-node bifurcation and Hopf bifurcation, respectively, for the rising phase of the input pass the threshold. After firing several spikes, the following falling phase drives the system into hyperpolarized state, whereby the neurons exhibit bursting behaviors (Fig. 4). However, the low-frequency sinusoidal input cannot drive class 3 neurons to displace the quasiseparatrix instantaneously for the slow rising phase. So the system emerges subthreshold oscillations. It is revealed that the class 3 neurons are more sensitive to the rising rate (slope) of the input. When the input frequency increases, one input cycle fires only one spike for three classes of neurons. Because there is not enough time to trigger more spikes for the depolarized segment, the coming hyperpolarization suppresses the membrane potential below the threshold. For the high-frequency stimuli, all the neurons produce subthreshold oscillations; thus, the output frequency falls to zero.

B. Synaptic input with determinate interspike interval distribution

In this subsection, we use the synaptic current described by the α function [14]. This α function synaptic input is close to physiological recordings of the postsynaptic response. The synaptic input equation is

$$I_{\text{ext}} = g_{\text{syn}} \sum_n \alpha(t - t_{i,n})(V_a - E_s). \tag{7}$$

Here g_{syn} is the conductance of the synapse controlling the synaptic input amplitude, and $t_{i,n}$ represents the start time of the nth presynaptic input pulse. The synaptic time delay is neglected. $V_a = 30$ mV is the maximal postsynaptic membrane potential, and $E_s = -50$ mV is the reversal potential of the synapse. The alpha function $\alpha(t)$ is defined by

$$\alpha(t) = (t/\tau)\, e^{-t/\tau}\theta(t), \tag{8}$$

where τ is the time constant relevant to synapse conduction and θ is the Heaviside step function. Note that this synaptic input here is essentially an α-shaped injection current with fixed amplitude, because the term $[V_a - E(s)]$ in Eq. (7) is constant. Although this form of input spike train is not what happens at a real synapse, it is convenient to modify the ISI of the input train. The ISI of input is given by

$$T_i = t_{i,n+1} - t_{i,n}, \tag{9}$$

where $t_{i,0} = 0$. The ISI of the synaptic input, in this subsection, is set to be deterministic, $T_i = T_{\text{const}}$. The input frequency is calculated by $f_{\text{in}} = 1/T_{\text{const}}$, and f_{in} and g_{syn} are set as free parameters.

Figure 5 (top panels) shows f_{out} as the function of f_{in} and g_{syn} in the form of a color map. The average output frequency f_{out} of class 1 and 2 neurons has nearly the same evolution properties driven by the synaptic stimuli with deterministic ISI inputs as varying synaptic conductivity g_{syn} and input frequency f_{in}, whereas class 3 neurons have a more complicated pattern. The output frequency f_{out} of all neurons increases with the input frequency f_{in}, and it appears to be 1 : 1 phase locked in a large parameter region. Here f_{out} decreases when f_{in} is larger than a certain value for a fixed g_{syn}. It is clear that a boundary separates the increasing area and decreasing area in Fig. 5 (top panels). In the high-input-frequency area,

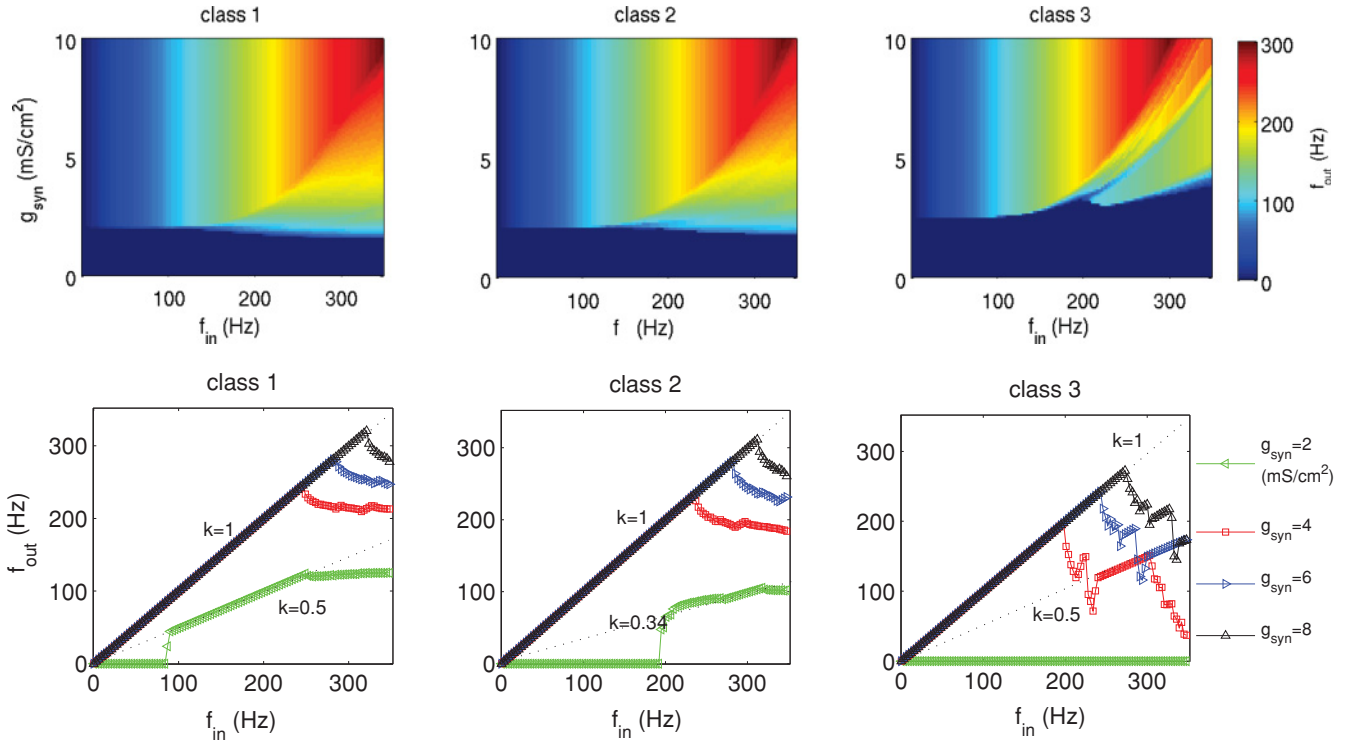

FIG. 5. (Color online) The average output frequency f_{out} of three classes of neurons driven by synaptic stimuli with dependent ISI inputs. Dotted curves in the bottom panels denote $k = f_{\text{out}}/f_{\text{in}}$.

the threshold (minimum conductivity leading neurons to fire action potentials) of class 1 and 2 neurons decreases, but for class 3 neurons, it increases.

The bottom panels in Fig. 5 show $f_{\rm out} \sim f_{\rm in}$ curves. All response frequencies are not larger than the input frequency. This means that all neurons do not exhibit bursting behaviors under dependent ISI synaptic input. When the conductivity $g_{\rm syn}$ is above the threshold, $f_{\rm out}$ increases linearly with $f_{\rm in}$. For high-frequency synaptic inputs, $f_{\rm out}$ begins to decrease, and the decreasing ratio is slow, unlike the case of high-frequency sinusoidal stimuli.

Here the postsynaptic current is more pulselike, and it is assumed that the α function has a high positive slope of rising phase and a slowly falling phase in a single-input pulse. When a low-frequency current is injected into the neurons and the synaptic conductivity is large enough, class 1 and 2 neurons were driven through the saddle-node bifurcation and Hopf bifurcation, respectively. These neurons exhibited only one action potential because the time of the input pulse duration was short. As for class 3 neurons, the system was driven through quasiseparatrix instantaneously and fires a spike, for the synaptic input with a high positive slope during the rising phase. Note that class 3 neurons are more sensitive to the slope of the input current to fire than the other two classes. For the refractory of the neurons, the higher the frequency of inputs, the more input pulses are filtered. On the other hand, high-frequency synaptic inputs easily drive the class 1 and 2 neurons across their bifurcations to initiate action potential spikes, thereby decreasing their thresholds. For class 3 neurons, a higher input amplitude is needed to drive the system to fire action potentials, or else the system will initiate a subthreshold oscillation. Therefore the threshold of class 3 neurons increases with the high-frequency input.

C. Synaptic inputs with random ISI distribution

In this subsection, the ISI of synaptic spike inputs T_i in Eq. (9) is assumed to be independent random variables with a Poisson distribution given by

$$P_p(x) = e^{-\lambda}\lambda^x/x! \quad (x = 0,1,\ldots). \tag{10}$$

Here x represents the random variables. Our calculations are performed by changing the mean ISIs, which is controlled by λ.

Figure 6 plots the ISI histogram of the neurons excited by a spike train with Poisson ISI distribution ($g_{\rm syn} = 3.0$ mS/cm^2, $\lambda = 3.5$ ms). Similarly, all neurons can filter the low ISIs. The output ISIs from three classes of neurons are no less than 5 ms, and the output ISIs of class 3 neurons are distributed in the largest region. One can clearly observe the low-pass filter behavior from the corresponding return maps in Fig. 7. Under low mean ISI input stimulation, class 3 neurons miss much more spikes than the other two classes; thus class 3 neurons have a much stronger ability to filter small-input ISIs. By increasing the mean ISIs, the output ISI histogram is similar to that of the input. This means that neurons fire synchronously with the input stimuli of a large value of mean ISIs.

It is helpful to use the information entropy to make clear the output ISI distribution property. For each spike train, we employ the normalized distribution of ISIs $P_{\rm ISI}(\Delta t)$, which

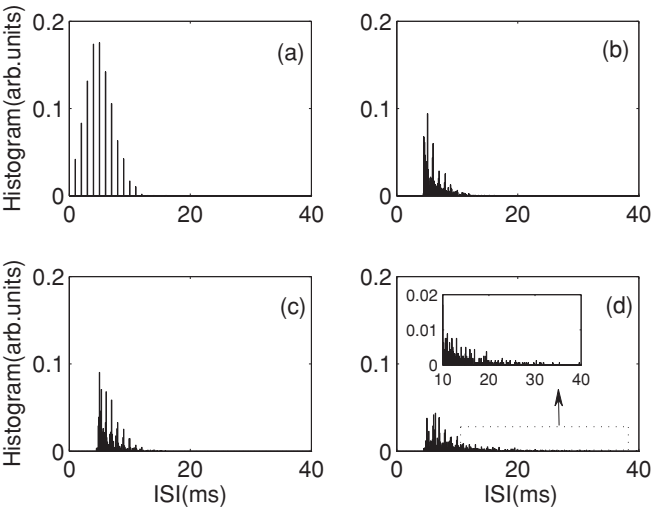

FIG. 6. The interspike intervals histogram of (a) synaptic input and output response of class 1 neuron (b), class 2 neuron (c), and class 3 neuron (d). Synaptic conductivity $g_{\rm syn} = 3.0$ mS/cm^2, $\lambda = 3.5$ ms. Inset of (d) is an enlarged view for the output ISI distribution in the insert.

denotes the probability of ISIs distributed between t and $t + \Delta t$. The entropy is defined as [22–24]

$$H = -\sum_{\text{observe}\,\Delta t} P_{\rm ISI}(\Delta t)\ln\left[P_{\rm ISI}(\Delta t)\right]. \tag{11}$$

The entropy here not only indicates the amount of information, but also illustrates the properties of ISI distributions.

In Fig. 8 we plotted the information entropy against the mean input ISIs λ. Under low λ, the response ISIs of class 3 neurons have the highest entropy. The entropies of class 1 and 2 neurons are both less than the entropy of the input spike train. As λ increases, the entropies of class 1 and 2 neurons increase, whereas the entropy of class 3 decreases then below the entropy of class 1. For λ above 7 ms, the entropy of class 3

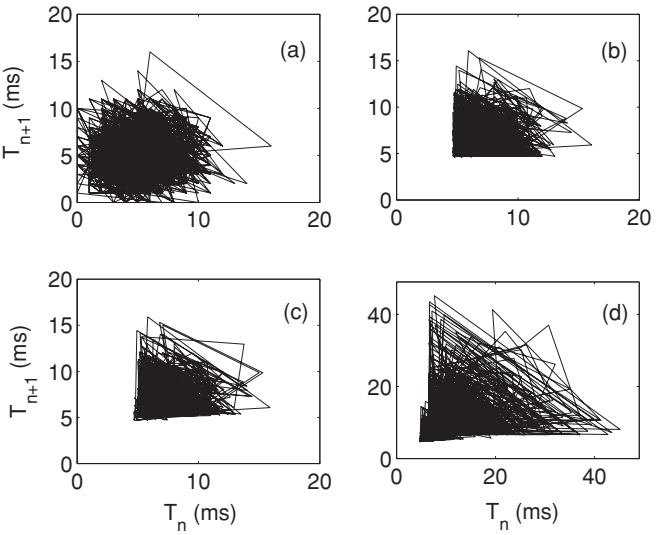

FIG. 7. ISI return maps of (a) synaptic input and output response of a class 1 neuron (b), class 2 neuron (c), and class 3 neuron (d). Synaptic conductivity $g_{\rm syn} = 3.0$ mS/cm^2, $\lambda = 3.5$ ms.

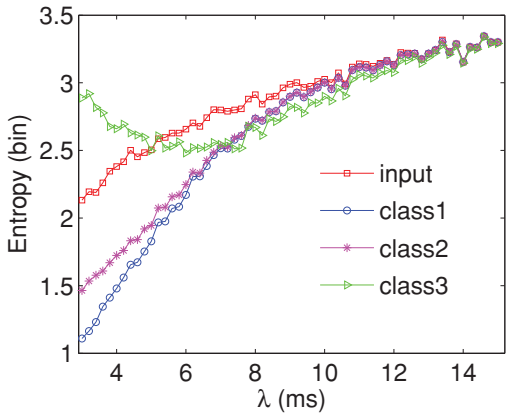

FIG. 8. (Color online) Information entropy of the spike-train inputs and the response spike trains of three classes of neurons against the mean values of input ISIs. The synaptic conductivity $g_{syn} = 3.5$ mS/cm^2.

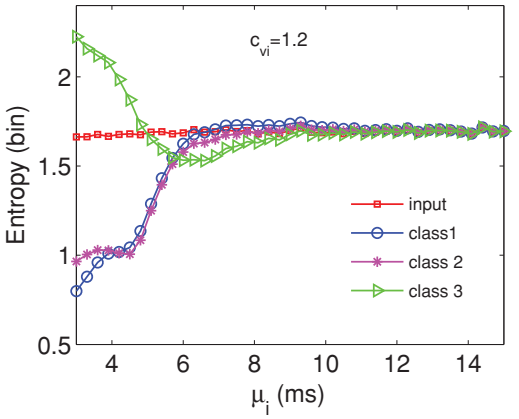

FIG. 9. (Color online) Information entropy of the spike-train inputs (red square) and the response spike trains of three classes of neurons (class 1: blue circle; class 2: magenta asterisk; class 3: green triangle) against the mean values of input ISIs. The synaptic conductivity $g_{syn} = 5$ mS/cm^2, variance of input spike train $c_{vi} = 1.2$.

neurons begin to increase with λ. Eventually the entropies of three classes of neurons get close to the input ISI entropy. This means that the output ISIs have the same distribution properties with input ISIs, when the high mean ISI λ input is injected into neurons.

The value of entropy is related to the form of the ISI distribution. A more concentrated distribution leads to a very low entropy; e.g. if $P_{\rm ISI}(\Delta t) = 1$ for a regular ISI distribution, then the entropy $H = 0$. When the mean input ISI is low, class 3 neurons expand the ISI distribution in a large region, while filtering the ISIs lower than 5 ms (see Fig. 6). Class 1 and 2 neurons filter more ISIs but hardly an expanded ISI distribution. Thus class 3 neurons have the highest entropy, and the entropies of class 1 and 2 neurons are less than the entropy of inputs. On the one hand, as the value of mean input ISIs increases, the number of low ISIs in the input train gets smaller; thereby all three classes of neurons filter a small amount of input ISIs, and the output ISI distribution become more similar to the input train. Thus, the entropy of three classes of neurons is close to the input entropy. Moreover, by increasing the mean input ISIs, the variance of input ISIs increases; thus the entropy of the input train as well as the entropies of three classes of neurons increases.

In order to separate the effects of mean and variance of random ISIs, we performed the simulation using input ISIs with a Gamma distribution. The Gamma probability density function is given by

$$P_g(x) = \frac{x^{\alpha-1}e^{-x/\beta}}{\beta^{\alpha}\kappa(x)} \qquad (x > 0). \tag{12}$$

Here, the mean value of input ISIs $\mu_i = \alpha\beta$, and variance of input ISIs $c_{vi} = \alpha\beta\beta$.

Figure 9 shown the information entropies changing with mean input ISIs. As μ_i is increasing, the entropies of three classes of neurons show evolutionary behaviors similar to that of Poisson distribution. In the case of low μ_i, the entropies of all classes are different. Increasing μ_i, the entropies of all three classes of neurons get close to the input ISI entropy.

With the same-input mean ISIs, the larger input variance yields larger output entropy. Figure 10 shows the entropies against the input variance c_{vi} with $\mu_i = 3.3$ ms, 11.1 ms. In the left panel of Fig. 10, the entropy of class 3 is largest and that of class 1 is lowest. With increasing c_{vi}, the entropies increase. For $\mu_i = 11.1$ ms all the output entropies of three classes of neurons are close to each other. As the input variance increases, the output entropies of all neurons increase sharply.

The output ISI distribution of three classes of neurons depends on the mean ISIs of the input train as well as their variance. This result is consistent with the outcome of Ref. [14], which focused only on class 2 neurons (HH model). Here we not only show the entropy of the neurons, but also reveal the properties of their output ISI distribution. All three classes of neurons fail to respond to all amounts of information of the low mean ISI inputs, class 3 with a higher entropy and classes 1 and 2 with a lower entropy than the inputs. For assembly of class 3 to class 1 or 2 neurons in a network would require full information of the input. This entropy evolution property reveals a potential useful coding mechanism for information transmission.

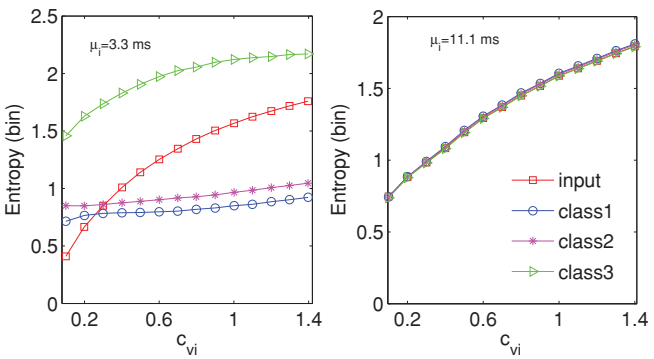

FIG. 10. (Color online) The entropies against variance c_{vi} for inputs with Gamma distribution ISI with the mean value $\mu_i = 3.3$ ms (left panel) and 11.1 ms (right panel).

IV. CONCLUSION

In this paper the responses of three classes of neurons to various types of inputs have been numerically investigated. We not only discussed the response of three classes of neurons to different types of inputs, but also analyzed the difference of the response properties among three classes. It was found, varying the input frequency and amplitude, that the output frequency responses of class 1 and 2 neurons show similar properties, whereas class 3 neurons display more complicated response behaviors.

Under sinusoidal stimuli, class 1 and 2 neurons show bursting behaviors in the low-input-frequency area, whereas class 3 neurons do not fire action potential in this input area even if the input amplitude is very high. This result is consistent with experimental evidence. Auditory brain stem neurons exhibit typical class 3 excitability and do not respond to a low-frequency sinusoidal current [25] and a slow-rising ramp current [26–28]. By increasing the input frequency, all neuron classes exhibit 1 : 1 phase-locking behavior. This phase-locking behavior produces an accurate firing response [19]. With increasing input frequency, the output frequency of three classes of neurons reduces to zero (subthreshold oscillation). The similar phase-locking behaviors are also observed in the case of deterministic ISI synaptic puleslike input. These increasing and decreasing behaviors of response frequency are consistent with the series of experiments of extracellular recordings [29]. In addition, the class 3 neuron is more sensitive to the slope of the input current than the other two classes. Recently, it has been reported that neurons encode the magnitude of input slope rather than input amplitude [30]. Previous experiments observed a similar result, where some cortex neurons are able to detect the slope of sensory signals [31,32].

Where mean ISI of random input is low, all three classes of neurons exhibit low-pass filter behavior. As mean ISI of random input increases, the output ISI histograms are more and more similar to that of the input. Clearly, in both the cases of Poisson and Gamma distribution ISI input, all three classes of neurons fail to respond to full information in the case of low mean ISI inputs. However, assembling class 3 to class 1 or 2 neurons in a network, it would be possible to respond to the full input information. Thus, we conjecture that this entropy property reveals a potential useful coding mechanism for information transmission.

V. ACKNOWLEDGMENTS

We very much appreciate two anonymous referees for their very constructive and helpful suggestions. This work was supported by the NSFC (Grant No. 10975063) and the Fundamental Research Funds for the Central Universities (Grant No. lzujbky-2009-52).

[1] R. Schmitt, P. Dev, and B. Smith, Science **193**, 114 (1976).
[2] Y. Pasztor and B. Bush, Science **215**, 1635 (1982).
[3] W. Gerstner, A. K. Kreiter, H. Markram, and A. V. M. Herz, Proc. Natl. Acad. Sci. USA **94**, 12740 (1997).
[4] F. Rieke, D. Warland, R. D. R. V. Steveninck, and W. Bialek, *Spikes: Exploring the Neural Code* (MIT Press, Cambridge, MA, 1999).
[5] P. Dayan and L. F. Abbott, *Theoretical Neuroscience: Computational and Mathematical Modeling of Neural Systems* (MIT Press, Cambridge, MA, 2001).
[6] N. Masuda and K. Aihara, Math. Biosci. **207**, 312 (2007).
[7] Y. Chen, L. Yu, and S.-M. Qin, Phys. Rev. E **78**, 051909 (2008).
[8] E. Kandel, J. Schwartz, and T. Jessell, *Principles of Neural Science* (McGraw-Hill Medical, New York, 2000).
[9] A. L. Hodgkin, J. Physiol. (London) **107**, 165 (1948).
[10] T. Tateno, A. Harsch, and H. P. C. Robinson, J. Neurophysiol. **92**, 2283 (2004).
[11] E. M. Izhikevich, *Dynamical Systems in Neuroscience: The Geometry of Excitability and Bursting* (MIT Press, Cambridge, MA, 2006).
[12] S. A. Prescott, Y. De Koninck, and T. J. Sejnowski, PLoS Comput. Biol. **4**, e1000198 (2008).
[13] J. R. Clay, D. Paydarfar, and D. B. Forger, J. R. Soc. Interface **5**, 1421 (2008).
[14] H. Hasegawa, Phys. Rev. E **61**, 718 (2000); **62**, 1456(E) (2000).
[15] J. C. Brumberg and B. S. Gutkin, Brain Res. **1171**, 122 (2007).
[16] Y. Che, J. Wang, W. Si, and X. Fei, Chaos Solitons Fractals **39**, 454 (2009).
[17] H. Gonzalez, H. Arce, and M. R. Guevara, Phys. Rev. E **78**, 036217 (2008).
[18] J. Laudanski, S. Coombes, A. R. Palmer, and C. J. Sumner, J. Neurophysiol. **103**, 1226 (2010).
[19] J.-M. Fellous, A. R. Houweling, R. H. Modi, R. P. N. Rao, P. H. E. Tiesinga, and T. J. Sejnowski, J. Neurophysiol. **85**, 1782 (2001).
[20] S. G. Lee and S. Kim, Phys. Rev. E **73**, 041924 (2006).
[21] L. S. Borkowski, Phys. Rev. E **80**, 051914 (2009).
[22] A. Borst and F. E. Theunissen, Nat. Neurosci. **2**, 947 (1999).
[23] H. D. I. Abarbanel and E. C. Tumer, *in Perspectives and Problems in Nonlinear Science. A Celebratory Volume in Honor of Lawrence Sirovich, Springer Applied Mathematical Sciences Series*, edited by E. Kaplan, J. E. Marsden, and K. R. Sreenivasan (Springer, Berlin, 2003).
[24] A. D. Dorval, J. Neurosci. Methods **173**, 129 (2008).
[25] M. Beraneck, S. Pfanzelt, I. Vassias, M. Rohregger, N. Vibert, P. Vidal, L. E. Moore, and H. Straka, J. Neurosci. **27**, 4283 (2007).
[26] D. Oertel, J. Neurosci. **3**, 2043 (1983).
[27] M. J. McGinley and D. Oertel, Hear. Res. **216–217**, 52 (2006).
[28] Y. Gai, B. Doiron, V. Kotak, and J. Rinzel, J. Neurophysiol. **102**, 3447 (2009).
[29] J. Kang, H. P. C. Robinson, and J. Feng, PLoS ONE **5**, e9608 (2010).
[30] A. Kepecs, X.-J. Wang, and J. Lisman, J. Neurosci. **22**, 9053 (2002).
[31] W. Metzner, C. Koch, R. Wessel, and F. Gabbiani, J. Neurosci. **18**, 2283 (1998).
[32] S. Sherman, Trends Neurosci. **24**, 122 (2001).